

High-Throughput Cellular Heterogeneity Analysis in Cell Migration at the Single-Cell Level

Mengli Zhou, Yushu Ma, Chun-Cheng Chiang, Edwin C. Rock, Kathryn E. Luker, Gary D. Luker, and Yu-Chih Chen*

Cancer cell migration represents an essential step toward metastasis and cancer deaths. However, conventional drug discovery focuses on cytotoxic and growth-inhibiting compounds rather than inhibitors of migration. Drug screening assays generally measure the average response of many cells, masking distinct cell populations that drive metastasis and resist treatments. Here, this work presents a high-throughput microfluidic cell migration platform that coordinates robotic liquid handling and computer vision for rapidly quantifying individual cellular motility. Using this innovative technology, 172 compounds were tested and a surprisingly low correlation between migration and growth inhibition was found. Notably, many compounds were found to inhibit migration of most cells while leaving fast-moving subpopulations unaffected. This work further pinpoints synergistic drug combinations, including Bortezomib and Danirixin, to stop fast-moving cells. To explain the observed cell behaviors, single-cell morphological and molecular analysis were performed. These studies establish a novel technology to identify promising migration inhibitors for cancer treatment and relevant applications.

cancer metastasis is a complicated multi-step process, migration and intravasation of tumor cells from the tumor stroma to a capillary bed or lymphatic vessel represent critical early steps.^[3] In addition, considerable evidence suggests that cancer metastasis can be driven by epithelial-to-mesenchymal transition (EMT),^[4–6] a developmental program in which epithelial cells acquire migratory and invasive phenotypes.^[7–10] Inhibition or activation of EMT significantly limits or increases metastasis, respectively.^[11–13] To elucidate the correlation between cancer migration and metastasis, we previously developed a high-throughput microfluidic platform that can measure the individual migratory capability of thousands of cancer cells and selectively isolate fast-moving subpopulations.^[14,15] As expected, we found that highly migratory breast cancer cells metastasized more than non-migratory

1. Introduction

Metastasis is the major cause of breast cancer deaths, accounting for over 40 000 deaths per year in the United States (US). Despite advances in early detection and treatment, once metastases develop, breast cancer remains incurable.^[1,2] While

cells.^[15] Furthermore, through whole transcriptome sequencing of migratory and control cancer cells, differentially expressed genes that correlate with clinical outcomes in breast cancer were identified.^[16] The distinct gene expression profile of migratory cancer cells highlights the possibility to selectively inhibit this metastatic sub-population. As migratory breast

M. Zhou, Y. Ma, C.-C. Chiang, Y.-C. Chen
UPMC Hillman Cancer Center
University of Pittsburgh
5115 Centre Ave, Pittsburgh, PA 15232, USA
E-mail: chen25@upmc.edu

M. Zhou, Y. Ma, C.-C. Chiang, Y.-C. Chen
Department of Computational and Systems Biology
University of Pittsburgh
3420 Forbes Avenue, Pittsburgh, PA 15260, USA

M. Zhou
Xiangya Hospital
Central South University
Changsha, Hunan 410008, China


E. C. Rock, Y.-C. Chen
Department of Bioengineering
Swanson School of Engineering
University of Pittsburgh
3700 O'Hara Street, Pittsburgh, PA 15260, USA

K. E. Luker, G. D. Luker
Center for Molecular Imaging
Department of Radiology
University of Michigan
109 Zina Pitcher Place, Ann Arbor, MI 48109-2200, USA

G. D. Luker
Department of Microbiology and Immunology
University of Michigan
109 Zina Pitcher Place, Ann Arbor, MI 48109-2200, USA

G. D. Luker
Department of Biomedical Engineering
University of Michigan
2200 Bonisteel, Blvd, Ann Arbor, MI 48109-2099, USA

Y.-C. Chen
CMU-Pitt Ph.D. Program in Computational Biology
University of Pittsburgh
3420 Forbes Avenue, Pittsburgh, PA 15260, USA

 The ORCID identification number(s) for the author(s) of this article can be found under <https://doi.org/10.1002/sml.202206754>.

DOI: 10.1002/sml.202206754

cancer cells are key contributors to metastatic dissemination, we expect that inhibition of cell migration can reduce the metastatic burden of breast cancer.^[15,17,18]

Despite the importance of cancer cell migration in metastasis, it has been neglected in conventional drug discovery. Conventional drug screening focuses mainly on compounds that significantly inhibit cell viability and/or growth.^[19] For instance, NCI-60 Human Tumor Cell Lines Screen first performed a one-dose assay to quantify growth inhibition and lethality of compounds. The compounds that do not exhibit significant growth inhibition were not considered further. However, compounds that inhibit cell migration might have potent clinical value for metastatic disease. While there are some previous trials targeting cell functions relevant to migration, including protease, integrin, and extracellular matrix (ECM), there is no systematic screening for cell migration inhibitors.^[20–25] More importantly, the screening experiments generally measure the responses of many cells in bulk, masking a small number of distinct cells that may drive metastasis.^[11–13]

Cellular heterogeneity is a hallmark of multicellular life which presents various forms and functions in organisms by facilitating specialization. This heterogeneity controls physiological processes of normal cells as well as pathological conditions of many diseases.^[26,27] However, most of our current biological knowledge is based on population-averaged measurements. While bulk analysis of many cells altogether measures the overall cellular responses, regulations and mechanisms, the baseline assumption that all cells are identical can lead to imprecise and often incorrect assessments.^[28] With new engineering tools having single-cell resolution, it has become clear that cell-to-cell variability is pervasive and critical.^[29] Cancer as a genetic disease has an abnormal and unstable genome and epigenome.^[30] The instability can be caused by erroneous DNA repair mechanisms and an abnormal tumor micro-environment, which is hypoxic, acidic, and lacks nutrition.^[31,32] This molecular-level instability leads to inter-patient and intra-patient tumor heterogeneity and generates formidable challenges in identifying optimal treatments.^[28,33,34]

Popular established cell migration assays, such as wound healing and transwells, have limited utility for detecting single-cell heterogeneity.^[35,36] Wound healing assays present challenges both in the reproducibility of the scratch and the difficulty tracking individual cells.^[37] Transwell assays provide a binary migration measurement of cells, but tracking the actual cell movement process is not possible. These fundamental limitations hinder the study of cellular heterogeneity and dynamics of cell migration. Due to the features of small reagent volumes, precise fluid control, and small device footprint, microfluidics has emerged as a cutting-edge technology to monitor the movement of individual cells.^[14–18,38–45] Despite significantly better single-cell tracking capability of microfluidic platforms, most existing devices are not readily compatible and coordinated with robotic liquid handling and image processing for high-throughput screening. To identify potent cell migration inhibitors and consider cellular heterogeneity, there is an unmet need to measure single-cell motility in high throughput and at low cost. To address the limitations of existing platforms, we developed a high-throughput microfluidic migration platform for tracking the movement of thousands of cells. We

focused on triple-negative breast cancer (TNBC), which is more aggressive and has few targeted therapies.^[46,47] Utilizing the cutting-edge screening capability of our system, we screened a custom library of 172 compounds to identify compounds that specifically inhibited cell migration, cell proliferation, or both. The experiments suggest that inhibition of cell migration and proliferation are not highly correlated, so conventional drug screening experiments might overlook promising migration inhibitors. In addition to the mean cell migration capacity, we characterized the movement of top-ranked fast-moving cells. Interestingly, we found many compounds that inhibited the migration of most cells but not fast-moving ones. The cellular heterogeneity would not be revealed without individual cell tracking. Based on the throughput of the presented method, we tested drug combinations to stop the movement of fast-moving cells. We also performed single-cell morphological and molecular characterization to explain the observed cell migration phenotype.

2. Results

2.1. High-throughput Microfluidic Migration Assay with Autonomous Image Processing

We developed a high-throughput microfluidic migration platform that can quantify the migration distance of 100 individual cells per condition and test 32 treatment conditions on a single device (**Figure 1A**). After the migration assay of 24 h, images were collected by a motorized Nikon Ti2-E fluorescence microscope. Based on our previously developed MATLAB program for quantifying cell migration, we further established an autonomous image processing toolkit with fully automatic image registration and quality control functions.^[15] The image registration was performed using two features on the images. 1) The blue auto-fluorescence of Silicone on the ProPlate 64-Well device was used to crop the region of cell migration channels. 2) The brightfield image of migration channels was used to calculate the rotation angles of images and separate individual channels (**Figure 1B**). Based on the two features, the images can be automatically rotated and cropped for analysis. In addition, we implemented quality control functions to exclude images from defective microfluidic devices and/or poor imaging conditions. The migration devices with leakage, trapped bubbles were excluded. The over-exposed and out-of-focus images were also eliminated automatically. After quality control and image processing, the locations of cells were calculated based on cellular fluorescence. Point noise, debris, and dead cells were excluded by their small area and/or dim fluorescence. It takes around 2 s to process an image. The enlarged images tracking the movement of individual cells are shown in **Figure S1**, Supporting Information. As a proof of the concept, we compared the presented microfluidics with conventional transwell assays using the same chemoattractant of serum. The side-by-side comparison highlights the advantages of the presented method. 1) The conventional transwell assay cannot clearly distinguish the effects of cell killing and migration inhibition. As a demonstration, we treated cells with a CD4/6 inhibitor (Abemaciclib) which inhibited cancer

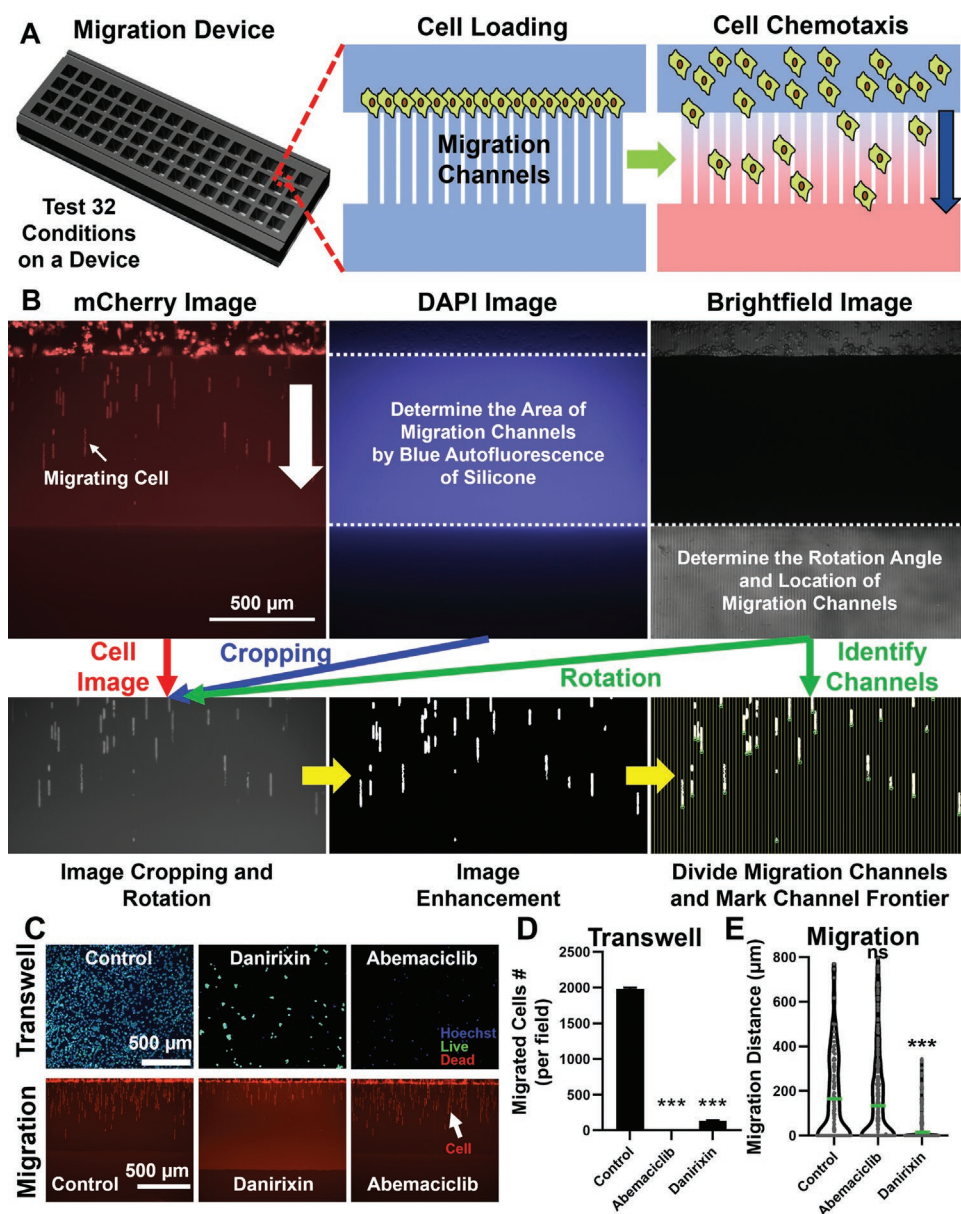


Figure 1. High-throughput microfluidic migration platform with single-cell resolution. A) A migration device that can test 32 conditions with 100 cells per condition. Two wells are used as a pair for cell migration analysis, and the cell migration channels are between two wells. Initially, cells are loaded into the upper wells. After cell adhesion, chemoattractant is loaded in the lower wells to induce cell migration into channels. B) The representative images of migrating cells, Silicone outline, and migration channels for image processing. Scale bar: 500 μm . C) The transwell and migration assays of MDA-MB-231 cells treated with DMSO control, Danirixin and Abemaciclib (10 μM for all compounds). Cells were stained with Live (green), Dead (red), and Hoechst (blue) staining reagents in the transwell experiments. Scale bar: 500 μm . D) The transwell assay of MDA-MB-231 treated with DMSO control, Danirixin and Abemaciclib. ($N = 3$) E) The microfluidic migration assay of MDA-MB-231 treated with DMSO control, Danirixin and Abemaciclib. $N = 300$ channels. Statistical analysis is provided in Tables S1 and S2, Supporting Information.

cell growth but did not stop cell migration and an IL8 inhibitor (Danirixin) which inhibited cell migration but not growth. Transwell assays showed negative for both treatments, yet the presented microfluidic migration assay detected the differences (Figure 1C–E, Tables S1 and S2, Supporting Information). 2) The microfluidic approach tracked the actual moving process of individual cells, so not only the mean cellular migration distance but also the migration distance of the top-ranked (*e.g.*, 95th percentile) fast-moving cells could be

measured. 3) The transwell inserts could only test 24 conditions in the area of a well-plate (455 mm^2 per condition), while the microfluidic assay tested 32 conditions in the area of a glass slide (59 mm^2 per condition). The presented system has significantly higher throughput and saves reagents. In addition, the device matches the pitch of 384-well plate, so it is fully compatible with robotic liquid handling. Using an OpenTrons OT-2 pipetting robot, it takes 1 min to load cells onto a device and 3 min to add drugs for testing 32 conditions (Video S1,

Supporting Information). The manual and robotic operations achieved similar experimental results (Figure S2, Supporting Information).

2.2. Correlation between Growth and Migration Inhibition

Using the new high-throughput migration platform, we characterized the changes in cell chemotaxis toward serum when treated with a custom library of 172 compounds, including conventional chemotherapeutics, ferroptosis inducers, and inhibitors of mitogen-activated protein kinase (MAPK), bromodomain and extra-terminal motif (BET), histone deacetylase (HDAC), poly (ADP-ribose) polymerase (PARP), human epidermal growth factor receptor 2 (HER2), proteasome, hypoxia-inducible factor (HIF), aldehyde dehydrogenase (ALDH), autophagy, transforming growth factor-beta (TGF- β), CDK4/6, epidermal growth factor receptor (EGFR), nuclear factor-kappa B (NF- κ B), CXCR1, CXCR4, IL8, rho-associated protein kinase (ROCK), colony-stimulating factor 1 receptor (CSF1R), proto-oncogene tyrosine-protein kinase Src, p21-activated kinase (PAK), Rac, Rho, CDC42, focal adhesion kinase (FAK), Wnt, aurora, and regulators of key cellular components, including mitochondria, microtubule, integrin, kinesin, and myosin with multiple breast cancer cell lines (Tables S3 and S4, Supporting Information). A compound concentration of 10 μ M was used in the screening experiments following the NCI-60 human tumor cell lines screen project. In addition to cell migration assays, conventional growth inhibition experiments were performed to quantify the growth inhibition and/or cytotoxicity effects of compounds for three TNBC cell lines (Figure 2A–D, Table S5, Supporting Information). Interestingly, we found a weak correlation between migration and growth inhibition (correlation coefficients of MDA-MB-231: 0.17, SUM149: 0.34, SUM159: 0.34). The growth inhibitors are not necessarily strong inhibitors of cell migration, and migration inhibitors might not stop cell growth. In addition to single-dose treatments, we further tested 5 concentrations of selected compounds to validate the screening experiment (Figure 2E,F). We found interesting compounds, including Danirixin (GSK1325756), an IL8 inhibitor, which inhibited cell migration significantly but not cell growth, and Abemaciclib, a CDK4/6 inhibitor, which stopped cell growth but not cell migration (Figure 2G,H). IL8 inhibitor (Aprepitant) and CDK4/6 inhibitors (Palbociclib HCl and Ribociclib) have consistent effects as Danirixin and Abemaciclib, respectively. Among the 172 tested compounds, 84 compounds significantly inhibited cell migration but not growth, 18 compounds significantly inhibited growth but not migration, and 56 compounds inhibited both growth and migration (Table S6, Supporting Information). There are also compounds that can inhibit both cell growth and migration, including all five proteasome inhibitors (Bortezomib, MG-132, Carfilzomib, Ixazomib, and Ixazomib Citrate), three Src inhibitors (Saracatinib, Tirbanibulin, and Dasatinib), and five ferroptosis inducers (Imidazole ketone erastin (IKE), RSL3, FINO2, ML162, and ML210) (Figure 2I). The difference in cell growth and migration inhibition highlights the possibility that screening of cell migration inhibition can provide a unique list of promising compounds in cancer treatment.

2.3. Pinpointing the Motility of Fast-Moving Cells

We further investigated the movement of highly migratory cells in addition to the mean cell motility. Overall, the mean cell migration distance was correlated with that of the top 5% fast-moving cells (correlation coefficients of MDA-MB-231: 0.57, SUM149: 0.85, SUM159: 0.85) (Figure 3A–D). When treating three TNBC cell lines with the 172 compounds, 62 compounds significantly inhibited mean cell migration but not fast-moving cells, 1 compound significantly inhibited the movement of fast-moving cells but not mean cell migration, and 78 compounds inhibited both (Tables S7 and S8, Supporting Information). For example, Ispinesib, a potent and specific inhibitor of kinesin spindle protein (KSP), significantly slowed the movement of most cells, yet a small number of cells remained migratory (Figure 3E).^[48] The same situation was observed in other compounds, including Daidzin, which is a natural organic compound from soybean leaves and known to reduce ovarian and breast cancer cell migration, and SBI-0206965, an autophagy inhibitor.^[49–51] In comparison, IL8 inhibitors, Danirixin and Aprepitant, and proteasome inhibitors, Carfilzomib and Bortezomib, inhibited the movement of all cells (Figure 3E).^[52–54] Measuring the average cell migration capacity using conventional bulk assays will not reveal these differences. In addition to single-dose treatment, we further tested five concentrations of selected compounds to validate the screening results. Abemaciclib neither inhibited the migration of mean nor fast-moving cells (Figure 3F), and Danirixin inhibited the migration of both mean and fast-moving cells (Figure 3G). More interestingly, CUDC-101, a potent multi-targeted inhibitor against HDAC, EGFR, and HER2, inhibited the migration of mean, but not fast-moving cells (Figure 3H).^[55] The in-depth comparison of the bulk cells versus top-ranked fast-moving ones highlights the issue of cellular heterogeneity, which has been largely overlooked in many conventional assays.

2.4. Dynamics of Cell Movement and the Treatment Combinations

In addition to a snapshot observation, the migration platform allows tracking of individual cells (Figure 4A). When watching the dynamics of movement, we found a small number of fast-moving cells significantly outperformed most slow-moving cells. In literature, those fast-moving cells are reported to be the key drivers of tumor initiation and metastasis.^[15,17,18] While Danirixin and Bortezomib significantly inhibited the mean cell migration distance, a small number of fast-moving cells continued moving forward (Figure 4A). The inability to stop those fast-moving cells could be explained by cancer cellular heterogeneity and the existence of redundant pathways to circumvent the drug targets.^[56] Given the limitation of mono-drug treatments, we explored the combination of drugs to completely stop highly migratory cells. We first tested the combination of the migration inhibitor of Danirixin and the growth inhibitor of Abemaciclib (Figure 4B). Overall, the effects were orthogonal: the cell motility largely depended on the concentration of Danirixin, and the cell viability mostly depended on the concentration of Abemaciclib. However, we observed a strong

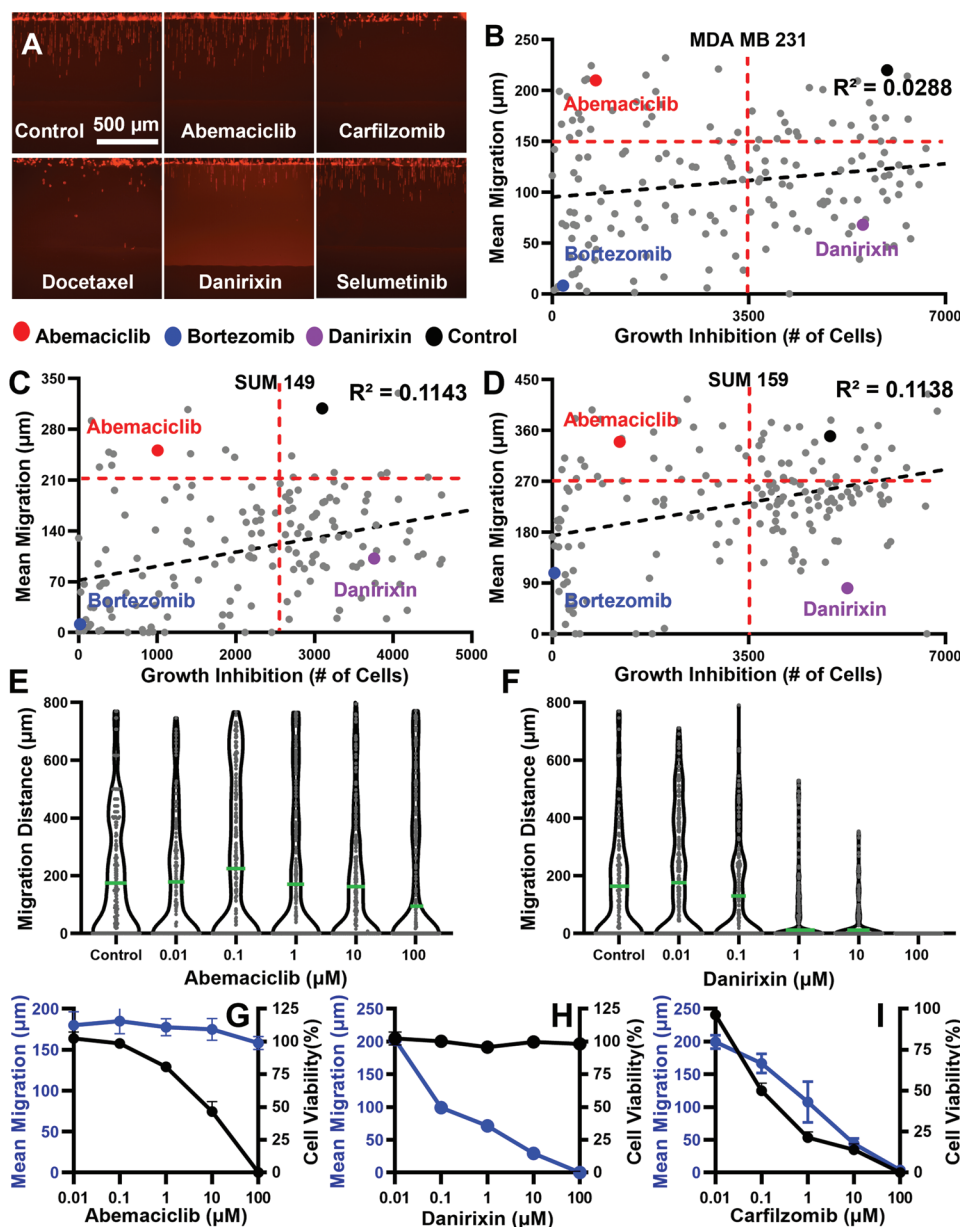


Figure 2. Correlation between the inhibition of cell growth and migration. A) Representative images of MDA-MB-231 cells treated with DMSO control, Abemaciclib, Carfilzomib, Docetaxel, Danirixin, and Selumetinib (10 μM for all compounds). Scale bar: 500 μm . B–D). Correlation between the inhibition of cell growth and migration for B) MDA-MB-231, C) SUM149, and D) SUM159 cell lines with Pearson's correlation coefficients: MDA-MB-231 ($R^2 = 0.0288$), SUM149 ($R^2 = 0.1143$), SUM159 ($R^2 = 0.1138$). The X-axis represents the number of cells after treatment, and the Y-axis represents the mean cell migration distance (μm). Each dot represents one compound. The red dot represents Abemaciclib treatment, the blue dot represents Bortezomib treatment, and the purple dot represents Danirixin treatment. Statistical analysis is provided in Tables S4 and S5, Supporting Information. E,F). Treatments of selected compounds (Abemaciclib and Danirixin) at 6 concentrations (100, 10, 1, 0.1, 0.01 μM , and DMSO control) on MDA-MB-231 cells. The X-axis represents the concentration of the compound, and the Y-axis represents cell migration distance. The green bars represent the mean cell motility. $N = 200$ channels. G–I) Treatments of selected compounds (Abemaciclib, Danirixin, and Carfilzomib) at five concentrations (100, 10, 1, 0.1, and 0.01 μM) on MDA-MB-231 cells. The Left Y-axis (blue) represents the migration distance, and the right Y-axis (black) represents the cell viability. The blue curve indicates the mean migration distance, and the black curve indicates the cell viability. Error bars indicate the standard error of the mean (SEM), $n = 3$.

synergistic effect on inhibiting cell migration when combining 1 μM of Danirixin and 10 μM of Abemaciclib. We also tested the combination of two cell migration inhibitors, Danirixin and Bortezomib. We found synergistic effects when combining 1–10 μM of Danirixin and 1–10 μM of Bortezomib (Figure 4C). The synergistic effects also exist for inhibiting fast-moving cells

(Figure S3, Supporting Information). When monitoring the cell movement over time (Figure 4A), we found that cell movement was completely stopped after 6 h by the combination of Danirixin and Bortezomib. The preliminary tests of drug combinations highlight the potential of the high-throughput platform to effectively examine combinations of compounds.

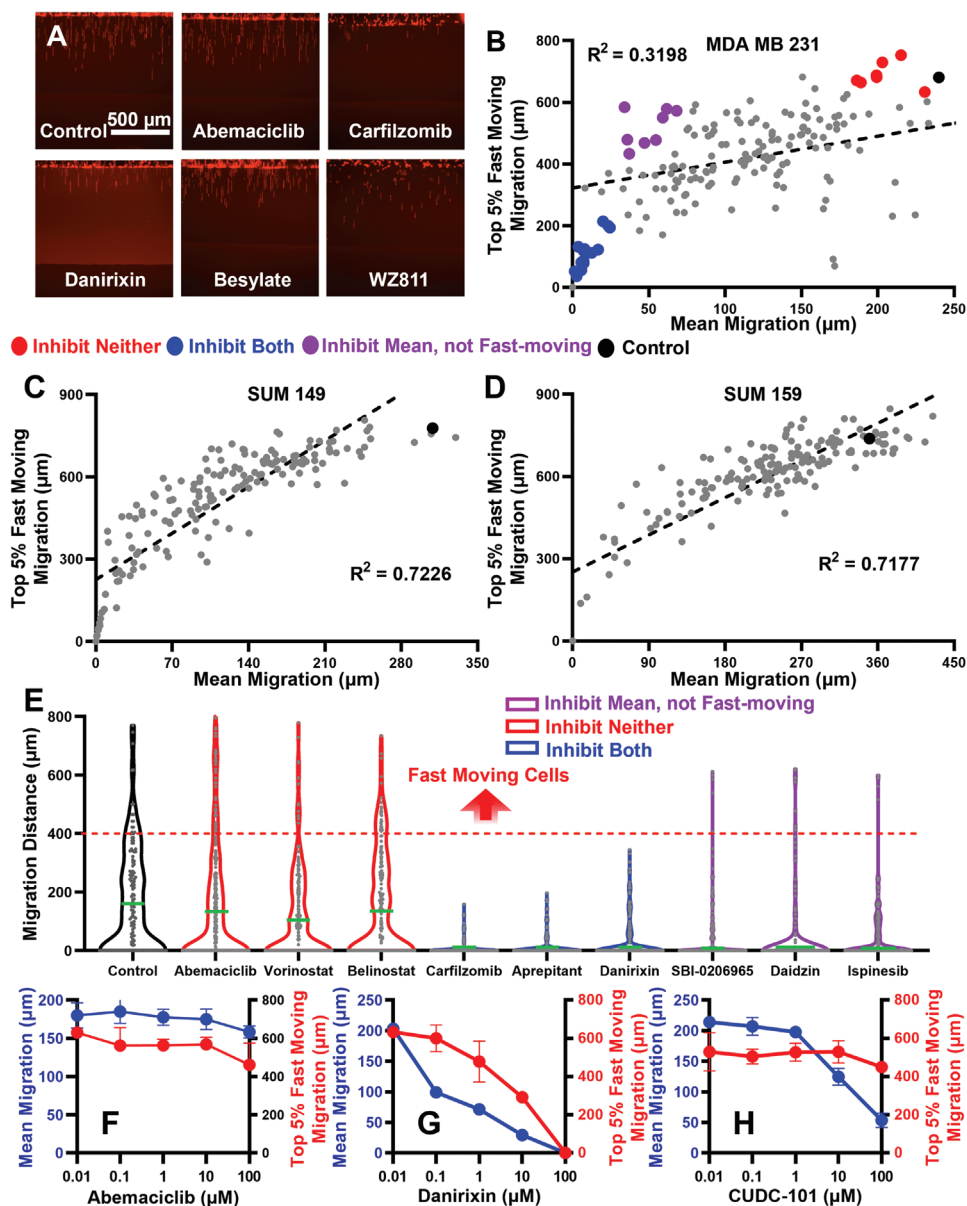


Figure 3. Correlation between the motility of mean and top-ranked fast-moving cells. A) Representative images of MDA-MB-231 treated with DMSO control, Abemaciclib, Carfilzomib, Danirixin, Besylate, and WZ811 (10 μM for all compounds). Scale bar: 500 μm . B–D). Correlation between the motility of mean and top-ranked fast-moving cells of B) MDA-MB-231, C) SUM149, and D) SUM159 cell lines with Pearson's correlation coefficients: MDA-MB-231 ($R^2 = 0.3198$), SUM149 ($R^2 = 0.7226$), SUM159 ($R^2 = 0.7177$). The X-axis represents the mean migration (μm) after treatment, and the Y-axis represents the top-ranked fast-moving migration distance (μm). Each dot represents one compound treatment. Different colors indicate different groups of compounds. The blue dots represent compounds that inhibited the migration of mean and top-ranked fast-moving cells, the red dots represent compounds that inhibited neither, the purple dots inhibited the migration of most cells but not the fast-moving ones, and the black dot represents DMSO control. Statistical analysis is provided in Table S7, Supporting Information. E) The distribution of migration distance for individual MDA-MB-231 cells treated with selected compounds (10 μM). The Y-axis represents cell migration distance. (μm). The green bars represent the mean cell motility. $N = 200$ channels. F–H) Treatments of selected compounds (Abemaciclib, Danirixin, and CUDC-101) at five concentrations (100, 10, 1, 0.1, and 0.01 μM) on MDA-MB-231 cells. The Left Y-axis (blue) represents the mean migration distance, and the right Y-axis (red) represents the top 5% fast-moving cell migration distance. (μm). Error bars indicate the standard error of the mean (SEM), $n = 3$.

2.5. Cellular Filopodia and Actin Morphology Correlate with Cell Motility

To better understand how cell migration was inhibited, we also examined the morphology of cellular actin and filopodia. Filopodia are composed of cross-linked actin microfilament

bundles and pioneer at the leading edge of migrating cells.^[57,58] Therefore, increased filopodia formation has been shown to promote migration.^[59] In our experiment, MDA-MB-231 cells were transfected with LifeAct-GFP for visualizing actin in filopodia. As shown in **Figure 5** and Table S9, Supporting Information, the number of filopodia significantly decreased with

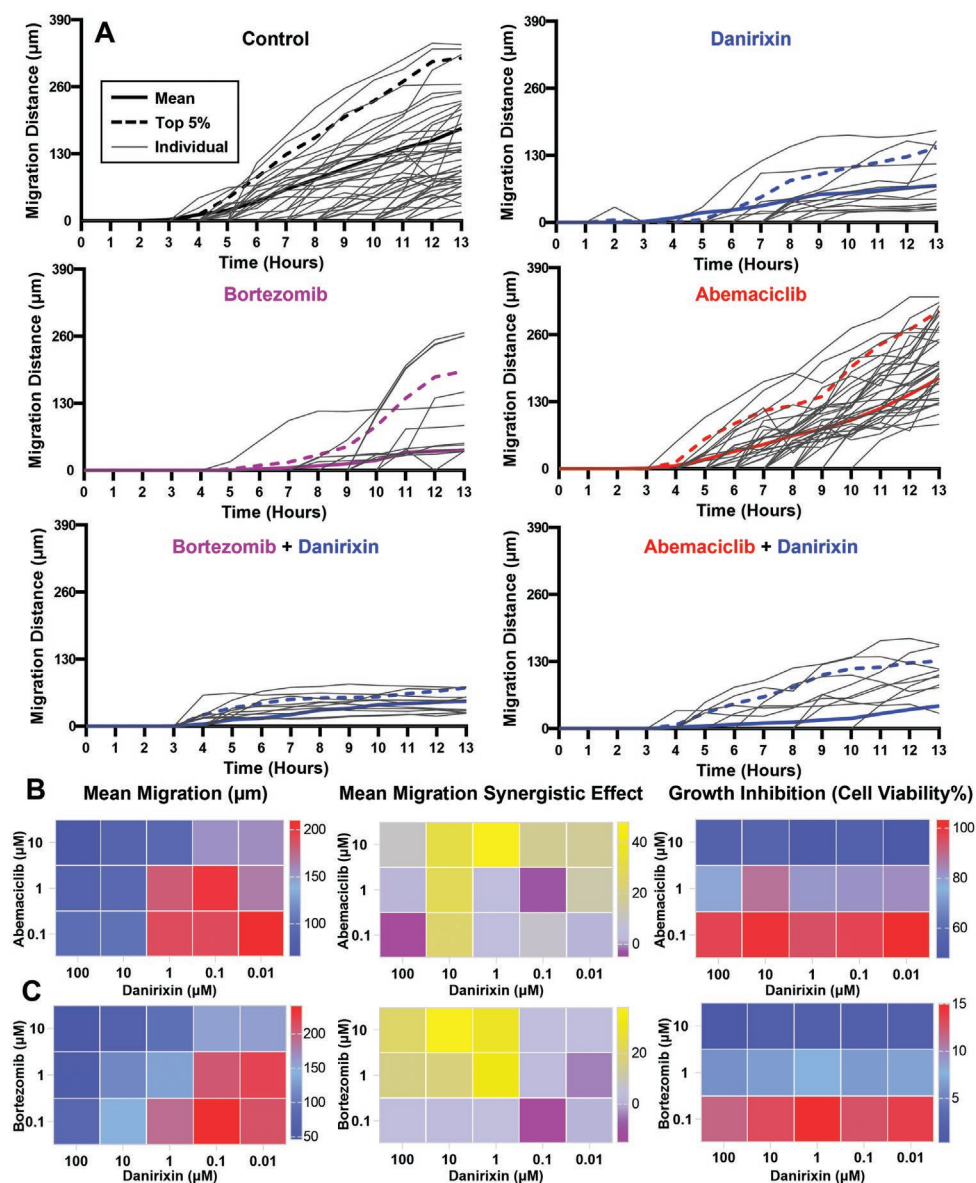


Figure 4. Dynamics of cell movement and the combination treatments of compounds. A) Dynamics of cell migration. MDA-MB 231 cells with selected compound treatments were imaged every hour for 13 h. The X-axis represents time (hours), and the Y-axis represents the migration distances (μm). The solid curve represents the mean migration distance, the dashed curve represents the top 5% fast-moving migration distance, and the gray thin solid curve represents the movement of individual cells. $N = 300$ channels. Six conditions of DMSO control, Danirixin, Bortezomib, Abemaciclib, Bortezomib+Danirixin, and Abemaciclib+Danirixin ($10 \mu\text{M}$ for all compounds) were tested. B,C). The combinatory effects on migration and cell viability. B) Abemaciclib C) Bortezomib at three concentrations (10, 1, and $0.1 \mu\text{M}$) combined with Danirixin at five concentrations (100, 10, 1, 0.1, and $0.01 \mu\text{M}$).

the treatment of Danirixin or Bortezomib. At the same time, Abemaciclib treatment does not alter the number of filopodia as compared to the control. The observation of cell morphology matches well with our prior data suggesting that Danirixin and Bortezomib inhibited cell migration, while Abemaciclib did not alter cell migratory behaviors although with high cytotoxicity.

2.6. Transcriptomic Effects of Abemaciclib

To better understand the unexpected effects of Abemaciclib, which inhibited cell growth but not migration, we performed

scRNA-Seq to profile molecular alterations by Abemaciclib. The control and treated MDA-MB-231 cells segregated well in the uniform manifold approximation and projection (UMAP) plot and by altered marker genes (Figure 6A,B). We identified the marker genes of Abemaciclib treatment and performed pathway analysis (Figure 6C,D). Using the NCI-Nature pathway database, two groups of pathways are highlighted: 1) cell cycle signaling, including “Aurora B,” “hepatocyte growth factor receptor,” and “C-MYC transcriptional activation” and 2) cell migration regulation, including “Posttranslational regulation of adherens junction,” “N-cadherin signaling,” “E-cadherin signaling,” “Nectin adhesion,” and “Integrin-linked kinase

A Control Abemaciclib Danirixin Bortezomib

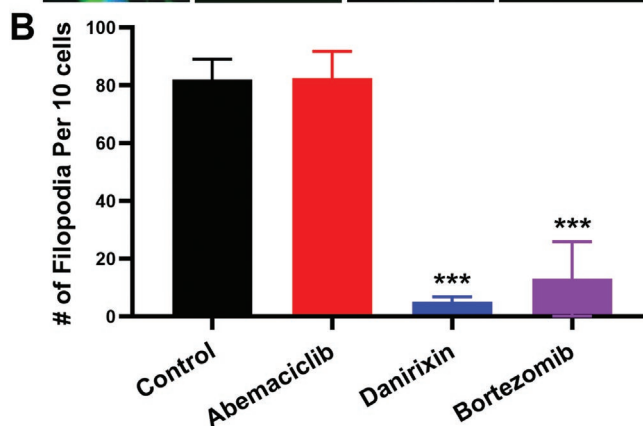
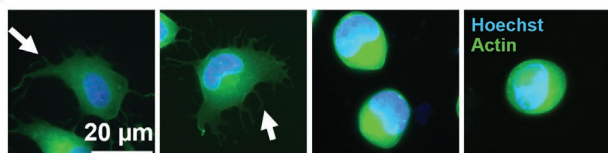


Figure 5. Cellular Filopodia are correlated with cell motility. A) Representative images of MDA-MB-231 cells treated with DMSO control, Abemaciclib, Danirixin, and Bortezomib (10 μm for all compounds). Blue fluorescence represents Hoechst staining, and green fluorescence represents GFP-Actin. Scale bar: 20 μm . B) The number of MDA-MB-231 cellular filopodia. The X-axis indicates the treatments. The Y-axis indicates the number of filopodia in every 10 cells. Statistical analysis is provided in Table S9, Supporting Information. *** refers to $p < 0.001$ Error bars indicate the standard error of the mean (SEM), $n = 4$.

signaling.” Using the GO Cellular Component pathway database, we also observed the activation of cell cycle related pathways of “nucleus” and “chromosome” and cell migration related pathways of “focal adhesion” and “cell-substrate junction.” The pathway analyses suggest that both cell cycle and migration are central to the difference between control and Abemaciclib treated cells. Specifically, Abemaciclib treatment significantly reduced the expression of key genes related to proliferation and cell cycle, including marker of proliferation Ki-67 (MKI67), DNA topoisomerase II alpha (TOP2A), centromere protein F (CENPF), Aurora Kinase A (AURKA), Cyclin B1 (CCNB1), Cyclin dependent kinase inhibitor 3 (CDKN3), pituitary tumor transforming gene 1 (PTTG1), protein disulfide-isomerase A3 (PDIA3), Chromobox 3 (CBX3) (Figure 6E).^[60–65] As such, the molecular changes match well with the observed cell growth inhibition by Abemaciclib and known effects of inhibiting CDK4/6. At the same time, treatment boosted the expression of migration related genes of Vimentin (VIM), cell division cycle protein 42 (CDC42), actin related protein 2/3 complex subunit 4 (ARPC4).^[66–69] More interestingly, the expression levels of key proteins in filopodia, including Ras Homolog Family Member A (RHOA), Ras Homolog Family Member C (RHOC), Actin Beta (ACTB), Rac Family Small GTPase 1 (RAC1), Myosins (percent.myo), Serpin Family E Member 1 (SERPINE1) remained comparable after treatment.^[70–75] The elevated and unchanged expression levels in key cell migration regulators match the observation that Abemaciclib treatment did not suppress cell migration. The preliminary investigation by scRNA-Seq explains the distinct effects of Abemaciclib on cell growth and migration.

3. Discussion

While the importance of cancer cell migration and heterogeneity has been widely acknowledged, there is no effective way to screen cell migration with single-cell resolution in high throughput. Although conventional migration assays (e.g., wound healing and transwell) are standardized for robotic operation, the assays are unable to track the movement of individual cells to study cellular heterogeneity. Microfluidic technology provides significantly better single-cell tracking capability, but most existing platforms are not readily compatible and coordinated with robotic liquid handling and image processing. In this work, we integrated user-friendly microfluidics, robotic liquid handling, and computer vision for a high-throughput migration assay at the single cell level. The platform is fully compatible with liquid handling systems. The robotic liquid handling can not only save time for researchers but also enhance the throughput and reproducibility of experiments. In addition to experiments, we establish an autonomous image processing toolkit with fully automatic image registration, quality control, and characterization of cell migratory behaviors. With the capability, we successfully analyzed thousands of images and tracked the movement of hundreds of thousands of individual cells. While we focus on breast cancer in this study, the established technology can be widely applied to other malignancies and applications related to cell migration.

In the comparison between inhibition of cell growth and migration, we found a strikingly weak correlation. The difference can be caused by technical reasons. For example, cell migration is a 1-day experiment, while cell growth experiments last 2 days. The differences in protocol naturally introduce inconsistency. At the same time, the scRNA-Seq experiment clearly supports the distinct molecular alteration of cell growth and migration by Abemaciclib. Within 1 day of treatment, Abemaciclib successfully suppressed the cell proliferation markers of MKI67 and TOP2A.^[61] The molecular changes match well with the observed growth inhibition. At the same time, the treatment enhanced the expression of VIM, CDC42, and ARPC4.^[66–69] Furthermore, the expression levels of many critical genes (e.g., RHOA, RHOC, and RAC1) in cell migration filopodia were not changed, which strongly support the unchanged cell migration capacity and filopodia morphology.^[70–74] The preliminary molecular investigation clearly supports that a compound can be a potent growth inhibitor but not a migration inhibitor. Given the importance of cell migration in the dissemination of cancer, the screening for cell migration inhibitors will provide an independent new list of promising compounds.

In addition to the average cell migration capacity, the platform also allows for the investigation of a small number of fast-moving cells. It was reported tens of tumor-initiating cells (TICs) are sufficient to generate a tumor in animal models.^[76–79] As such, reducing the migration capacity of most cells might not be sufficient to stop cancer metastasis. In our experiments, we found that many compounds significantly inhibited the average cell motility but not the fast-moving cells, especially for the MDA-MB-231 cell line, which is known to be highly aggressive and heterogeneous.^[80–82] The inability to stop those fast-moving cells might be explained by cancer cellular heterogeneity and the existence of redundant pathways. In our

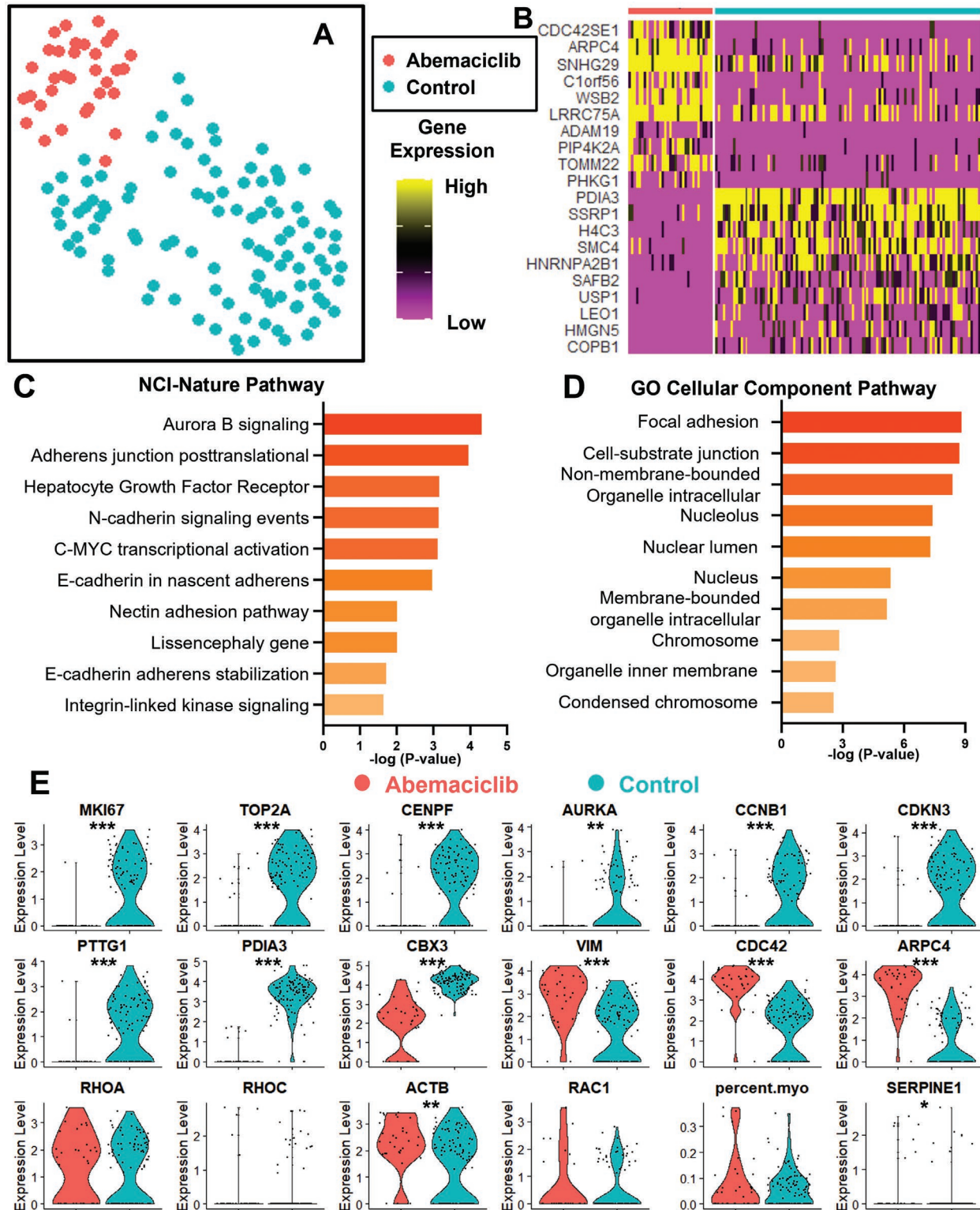


Figure 6. Single-cell transcriptome analysis of MDA-MB-231 with or without Abemaciclib treatment. A) UMAP plot of single-cell transcriptome analysis, MDA-MB-231 cells with and without Abemaciclib treatment. The X-axis represents UMAP1, the Y-axis represents UMAP2, and each dot represents one cell. Blue dots represent 105 control untreated cells, and red dots represent 33 Abemaciclib treated cells. B) Heatmap demonstrates the significant gene expression differences between treated and untreated MDA-MB-231 cells. C,D). Top-ranked pathways determined by the altered genes of MDA-MB-231 cells treated with Abemaciclib versus control. The X-axis and color represent the p -values, and the Y-axis indicates the names of pathways. C) The NCI-Nature pathway database and D) the GO Cellular Component pathway database. E) Violin plots of Abemaciclib treated and control MDA-MB-231 cells with statistical tests. The Y-axis represents gene expression with a logarithmic scale. Each dot represents one cell. * refers to $p < 0.05$. ** refers to $p < 0.01$, and *** refers to $p < 0.001$.

prior work, we have performed scRNA-Seq for highly migratory breast cancer cells.^[16] While migratory cells overall demonstrate an EMT-like gene expression profile, further interrogation of migratory cells reveals discrete sub-populations expressing epithelial (CDH1, EpCAM, and cytokeratins) or mesenchymal (CDH2, VIM, SNAI2, and ZEB1) markers. Co-existence of multiple cell states within the migratory population highlights the existence of multiple layers of cellular heterogeneity. In addition to the cellular heterogeneity in motility, migratory cells can become migratory based on different molecular mechanisms. Thus, it is essential to consider the combination of multiple inhibitors to stop distinct sub-populations of migratory cells. In this study, we performed preliminary tests to identify the synergistic combination of Danirixin and Bortezomib, which could stop the movement of all cells. The combination suppressed the potential alternative and/or redundant pathways to activate cell migration and inhibits all migratory sub-populations. To identify appropriate drug combinations in the future, it is necessary to include more candidates. The high throughput of the presented method would be the key to overcoming the experimental complexity and cost which increase exponentially.^[83–86]

4. Experimental Section

Cell Culture: MDA-MB-231 cells were cultured in Dulbecco's modified eagle medium (DMEM, Gibco 11 995) supplemented with 10% fetal bovine serum (FBS, Gibco 16 000), 1% GlutaMax (Gibco 35 050), 1% penicillin/streptomycin (pen/strep, Gibco 15 070), and 0.1% of plasmocin (InvivoGen ant-mpp). SUM149 and SUM159 cells were cultured in F-12 (Gibco 11 765) media supplemented with 5% FBS (Gibco 16 000), 1% pen/strep (Gibco 15 070), 1% GlutaMax (Gibco 35 050), 1 $\mu\text{g mL}^{-1}$ hydrocortisone (Sigma H4001), and 5 $\mu\text{g mL}^{-1}$ insulin (Sigma I6634), and 0.1% of plasmocin (InvivoGen, ant-mpp). MDA-MB-231, SUM149, and SUM159 cells were obtained from Dr. Gary Luker's lab at the University of Michigan. All cells were maintained at 37 °C in a humidified incubator with 5% CO₂. All the cells were cultured and passaged when the cells reached over 80% confluency in the dish.

Cell Transfection: TNBC cells were stably transfected using Xfect Transfection Reagent (Takara 631 317) with 5 μg of pEF1alpha-Tomato Vector plasmid (Takara 631 975). The cells labeled with red fluorescent proteins could be tracked for migration. The transfected cells were selected using G418 (Takara 631 307) treatment and sorted by flow cytometry for red fluorescence. Cells stably transduced with LifeAct-GFP were previously described to visualize actin.^[75,87]

Microfluidic Chip Design and Fabrication: The migration devices were fabricated from a single layer of PDMS (Polydimethylsiloxane, Sylgard 184, Dow Corning), which was fabricated on a silicon wafer by standard soft lithography. One mask was used to fabricate the migration channel (5 μm height). One device contains 3200 migration channels (100 channels per pair of wells), and the migration channel is 10 μm in width, 5 μm in height, and 1 mm in length. The size of a device is 75.8 mm by 25 mm, and the pitch between wells is 4.5 mm (following the 384-well plate format). The microfabrication was performed by MuWells Inc. The patterned PDMS layer was bonded to the ProPlate 64-Well Chambers (246 855, Grace Bio-Labs) after being activated by oxygen plasma treatment (Plasma Oven, PDC-001, Harrick Plasma) for 5 min to form a complete fluidic channel. After bonding, the devices were heated at 80 °C for 15 min to ensure bonding quality. The microfluidic chips were sanitized by UV radiation prior to use to ensure sterile conditions. Before cell loading, collagen (1.45 mL collagen (collagen Type 1, 354 236, BD Biosciences), 0.1 mL acetic acid in 50 mL DI water) was coated overnight on the device to enhance cell adhesion. Devices were then rinsed with cell culture media before usage to remove the residual collagen solution.

Cell Migration Assay: A library of 172 compounds was selected for the screening experiments based on their functions in literature as listed in Table S3, Supporting Information. The compounds were dissolved to 10 mM in either DMSO or PBS according to the instructions from the vendors. Compound solutions were prepared by serial dilution, and the final concentration of 10 μM was used in the screening experiments. DMSO (0.01%) treatment was used as the control. Cells were harvested from culture plates with 0.05% Trypsin/EDTA (Gibco, 25 200) and centrifuged at 1000 rpm for 4 min. Then, the cells were resuspended in culture media to a concentration of 4.17×10^5 cells mL^{-1} (2.5×10^4 cells per well). 60 μL of this cell suspension was pipetted into the upper wells and 20 μL of culture media was pipetted into the lower wells. Trypsinized rounded cells (diameter: 10–15 μm) were larger than the migration channel height (5 μm), so they were initially trapped at the entrance of migration channels. The device maintained a static flow condition and stayed in an incubator for 30 min to enhance cell adhesion on the substrate, and cell adhesion morphology was visually confirmed before doing the next step. After visual inspection, cell suspension in the upper wells was aspirated and replaced with 60 μL serum-free culture media with treatment compounds (10 μM). The lower wells would be added to 60 μL serum culture media with treatment compounds (10 μM) to induce chemotactic migration toward serum. Due to the nature of diffusion, the concentration of the chemoattractant in the migration channel increases linearly along the channel from the cell loading side. The detailed simulation and measurement were discussed in the previous works.^[14,15] Then, the device was put into a cell culture incubator. Migration distance was measured based on the final cell frontier (the cell migrating the farthest) of each migration channel after 24 h of incubation without media replenishment.

Growth Inhibition Assay: Cells were harvested from cell culture dishes with 0.05% Trypsin/EDTA (Gibco 25 200) and centrifuged at 1000 rpm for 4 min. Then, the cells were re-suspended in the cell culture media for seeding into 96-well plates. For SUM149 cells, 2000 cells in 100 μL media were seeded per well. For SUM159 and MDA-MB-231 cells, 1000 cells in 100 μL media were seeded per well. Loaded cells were cultured for 24 h and then treated with compounds for 48 h. Cells were then stained by 0.8 μM Calcein AM, 1.6 μM Ethidium homodimer-1 (Invitrogen L3224 Live/Dead Viability/Cytotoxicity Kit), and 5 μM Hoechst 33 342 (Thermo Scientific 62 249) for 30 min in the incubator and imaged. The Hoechst staining image was first filtered by top-hat and bottom-hat filters to reduce the background, enhanced by contrast adjustment, and binarized to quantify the size of nuclei. Cell debris were excluded by their smaller sizes. Live/Dead staining was used to exclude dead cells with dim live signals and bright dead signals. The custom MATLAB program for cell counting was developed based on the previous works.^[88,89]

Transwell Assay: Nunc Polycarbonate Cell Culture Inserts, 8 μm pore size (Thermo Scientific 140 644) were used for Transwell migration assays. Cell culture media (2 mL per well) with serum was added to 6-well plates, and 7.5×10^4 cells in 1 mL of serum-free media were added to Transwell inserts. After 30 min, compound treatments of 10 μM were applied. Then, the Transwell plate was put into a cell culture incubator. After 24 h, cells on the lower surface of the inserts were stained with 5 μM Hoechst 33 342 (Thermo Scientific 62 249), 0.8 μM Calcein AM (Invitrogen L3224) for 30 min. After washing three times with PBS (Gibco 10 010) to eliminate cells on the top surface and the residual dye, the inserts were observed and photographed under a microscope.

Image Acquisition: The microfluidic chips were imaged using an inverted microscope (Nikon Ti2-E). The brightfield and fluorescence images were taken with a 40 \times , 10 \times , or 4 \times objective lens and a monochrome CMOS camera (Hamamatsu ORCA-Fusion Gen-III sCMOS Camera). The field of view was around 14 mm², which could cover 100 cell migration channels in an image. The outline of the device was fluorescently imaged by a DAPI filter set, transfected RFP cells were fluorescently imaged by a mCherry filter set, and Actin-GFP cells were imaged by a FITC filter set. Auto focusing was performed to ensure the image remained in focus throughout the imaging experiments. It takes less than 10 min to image a migration device that tests 32 conditions. The time-lapse experiments to monitor cell

population dynamics were performed using a Tokai Hit stage top environment control on the Nikon Ti2-E microscope.

Autonomous Image Analysis for Monitoring Cellular Migration: To process thousands of images in this study, an autonomous image processing toolkit (MATLAB 2021b) was established with fully automatic image registration and quality control functions. The image registration was performed using two features on the images. 1) The blue auto-fluorescence of Silicone on the ProPlate 64-Well device was used to identify the region of cell migration channel. 2) The brightfield image of migration channels was used to calculate the rotation angles and separate individual channels. (Figure 1) As the patterns of migration channels extend beyond the core cell migration area, the patterns were recognizable by brightfield imaging. Based on those two features, the images could be automatically cropped and rotated for registration. In addition, quality control functions were implemented to exclude images from defective microfluidic devices and poor imaging conditions. The migration devices with leakage, trapped bubbles were excluded. The over-exposed and out-of-focus images were also eliminated automatically. On average, around 20% of images were excluded. After quality control, the migration channels were identified, and the location of cells was calculated based on cellular fluorescence. Point noise, debris, and dead cells were excluded by their small area and dim fluorescence. In each migration channel, the program marked the live cells that move farthest as the migration frontier in that channel. The software was validated by comparing manual and computer-aided cell identification. The autonomous image analysis successfully excluded all defective images, and the location of recognized cells was consistent with the manual identification.

Single-Cell RNA-Seq: High-throughput single-cell barcoding transcriptome sequencing was performed for MDA-MB-231 cells with and without Abemaciclib treatment.^[90–92] Cells were cultured in a 6-well plate (Corning 3516), treated with Abemaciclib for 24 h (the same as the migration experiment), and harvested with 0.05% Trypsin/EDTA (Gibco 25 200) for scRNA-Seq. It was aware that the microenvironment in the microfluidic channels was not the same as that in a 6-well plate. However, as it was difficult to retrieve cells directly from the enclosed migration channels, treated and untreated cells were cultured in a 6-well plate for side-by-side comparison. Cells and beads were paired in microwells, so the mRNA from lysed cells could hybridize onto the barcoded beads. After barcoded beads captured cellular mRNA, RT (ThermoFisher Maxima RT kit), PCR (Kapa HiFi Hotstart PCR Readymix), and library preparation (Illumina Nextera XT Library Prep Kit) were performed. The cDNA samples were then quantified and pooled by the UPMC Cancer Genome Core for sequencing using the Illumina NextSeq. ≈10 million paired-end reads (Read 1: 30 base pairs for the barcode and Read 2: 250 base pairs for mRNA read alignment) were obtained for each population. Reads were aligned using STAR with GRCh38.p13 Human reference genome and processed by the standard Dropseq 2.5.1 pipeline. Then, the open-source SEURAT 4.0 (<http://satijalab.org/seurat/>) was used to analyze single-cell sequencing data.^[93] Cells with more than 500 genes detected were considered successfully sequenced, and the cells having more than 5% mitochondrial gene expression were discarded for their poor viability.

Statistical Analysis: Statistical analysis was performed using R (version 4.1), GraphPad Prism 9, Combenefit (version 2.021), and MATLAB. Half-maximal inhibitory concentrations (IC50s) were determined using GraphPad Prism 9 software. Comparisons of two different groups were performed by the two-tailed Student's *t*-test. Multiple groups were compared using 2-way ANOVA (cell line and treatment condition are two variables) Fisher's least significant difference (LSD) test. Synergistic effects were calculated using the Combenefit software.^[94] The exact statistical setups were determined depending on the variable types and nature of analysis. Value of $p < 0.05$ was used to define statistically significant differences for all analyses. * refers to $p < 0.05$, ** refers to $p < 0.01$, and *** refers to $p < 0.001$. Standard error of the mean (SEM) was used for designating error bars. The number of samples or groups used was provided in the Figure Captions. The correlation coefficients were calculated based on the Pearson correlation using GraphPad Prism. For measurements with high variability (such as gene

expression levels), these data were compared on a log scale. For single-cell transcriptome sequencing data, the R package SEURAT was used for data analysis, such as outlier detection, hierarchical clustering, principal component analysis, and UMAP.^[93] To compare cell populations, altered genes defined by logarithmic fold change of 0.25 and the minimal portion of expressing cells of 10% for pathway analysis was identified. Pathway analysis was performed using Enrichr (<http://amp.pharm.mssm.edu/Enrichr/>) tool with the GO Cellular Component and NCI-Nature databases.^[95] The *p*-values in pathway analysis were generated using Fisher exact tests by Enrichr.

Supporting Information

Supporting Information is available from the Wiley Online Library or from the author.

Acknowledgements

This study was generously supported by start-up funding from the UPMC Hillman Cancer Center, the Women's Cancer Research Center (WCRC) at Magee Women's Research Institute, and the Pitt CTSI Pilot project (This project was supported by the National Institutes of Health through Grant Number UL1TR001857.) to Y.-C.C. M.Z. was partially supported by the Xiangya visiting scholar program. G.D.L. acknowledges funding from US NIH grants R01 CA238023, U24 CA237683, R01 CA238042, U01 CA210152, R33 CA225549, and R37 CA222563. K.E.L. acknowledges funding from R50 CA221807. G.D.L. and K.E.L. also acknowledge funding from the W.M. Keck Foundation. The authors thank the Nanoscale Fabrication Characterization Facility of the University of Pittsburgh (Pittsburgh, PA) for device fabrication and Drs. Adrian Lee and Steffi Oesterreich (University of Pittsburgh) for insightful discussion. [Correction added after publication 8 February 2023: The author name "Chun-Cheng Chiang" was corrected.]

Conflict of Interest

The authors declare no conflict of interest.

Author Contributions

M.Z. and Y.-C.C. performed the fabrication of microfluidic devices. M.Z. and Y.-C.C. performed the cell migration experiments. Y.M. developed the software for image processing. C.-C.C. and Y.-C.C. performed the single-cell RNA-Seq experiments. E.C.R. and Y.-C.C. performed the sequencing read alignment and data analysis. K.E.L., G.D.L., and Y.-C.C. performed cell transfection and transduction. Y.-C.C. supervised the study. M.Z., and Y.-C.C. wrote the manuscript. All authors discussed the results and commented on the manuscript.

Data Availability Statement

The data that support the findings of this study are available in the supplementary material of this article.

Keywords

breast cancer, cell migration, image processing, metastasis, microfluidics, single-cell analysis

Received: November 1, 2022
Published online: November 30, 2022

- [1] D. Hanahan, R. A. Weinberg, *Cell* **2011**, *144*, 646.
- [2] P. S. Steeg, *Nat. Med.* **2006**, *12*, 895.
- [3] J. J. Bravo-Cordero, L. Hodgson, J. Condeelis, *Curr. Opin. Cell Biol.* **2012**, *24*, 277.
- [4] N. Y. Frank, T. Schatton, M. H. Frank, *J. Clin. Invest.* **2010**, *120*, 41.
- [5] A. Kreso, J. E. Dick, *Cell Stem Cell* **2014**, *14*, 275.
- [6] M. D. Brooks, M. L. Burness, M. S. Wicha, *Cell Stem Cell* **2015**, *17*, 260.
- [7] S. A. Mani, W. Guo, M.-J. Liao, E. Ng. Eaton, A. Ayyanan, A. Y. Zhou, M. Brooks, F. Reinhard, C. C. Zhang, M. Shipitsin, L. L. Campbell, K. Polyak, C. Brisken, J. Yang, R. A. Weinberg, *Cell* **2008**, *133*, 704.
- [8] X. Ye, W. L. Tam, T. Shibue, Y. Kaygusuz, F. Reinhardt, E. Ng Eaton, R. A. Weinberg, *Nature* **2015**, *525*, 256.
- [9] X. Ye, R. A. Weinberg, *Trends Cell Biol.* **2015**, *25*, 675.
- [10] E. Lee, J. Wang, K. Yumoto, Y. Jung, F. C. Cackowski, A. M. Decker, Y. Li, R. T. Franceschi, K. J. Pienta, R. S. Taichman, *Neoplasia* **2016**, *18*, 553.
- [11] W. Guo, Z. Keckesova, J. L. Donaher, T. Shibue, V. Tischler, F. Reinhardt, S. Itzkovitz, A. Noske, U. Zürcher-Härdi, G. Bell, W. L. Tam, S. A. Mani, A. van Oudenaarden, R. A. Weinberg, *Cell* **2012**, *148*, 1015.
- [12] S. S. Roy, V. K. Gonugunta, A. Bandyopadhyay, M. K. Rao, G. J. Goodall, L.-Z. Sun, R. R. Tekmal, R. K. Vadlamudi, *Oncogene* **2014**, *33*, 3707.
- [13] H. D. Tran, K. Luitel, M. Kim, K. Zhang, G. D. Longmore, D. D. Tran, *Cancer Res.* **2014**, *74*, 6330.
- [14] Y.-C. Chen, S. G. Allen, P. N. Ingram, R. Buckanovich, S. D. Merajver, E. Yoon, *Sci. Rep.* **2015**, *5*, 9980.
- [15] Y.-C. Chen, B. Humphries, R. Brien, A. E. Gibbons, Y.-T. Chen, T. Qyli, H. R. Haley, M. E. Pirone, B. Chiang, A. Xiao, Y.-H. Cheng, Y. Luan, Z. Zhang, J. Cong, K. E. Luker, G. D. Luker, E. Yoon, *Sci. Rep.* **2018**, *8*, 244.
- [16] Y.-C. Chen, S. Sahoo, R. Brien, S. Jung, B. Humphries, W. Lee, Y.-H. Cheng, Z. Zhang, K. E. Luker, M. S. Wicha, G. D. Luker, E. Yoon, *Analyst* **2019**, *144*, 7296.
- [17] C. L. Yankaskas, K. N. Thompson, C. D. Paul, M. I. Vitolo, P. Mistriotis, A. Mahendra, V. K. Bajpai, D. J. Shea, K. M. Manto, A. C. Chai, N. Varadarajan, A. Kontogianni-Konstantopoulos, S. S. Martin, K. Konstantopoulos, *Nat. Biomed. Eng.* **2019**, *3*, 452.
- [18] B. S. Wong, S. R. Shah, C. L. Yankaskas, V. K. Bajpai, P.-H. Wu, D. Chin, B. Ifemembi, K. Refaey, P. Schiapparelli, X. Zheng, S. S. Martin, C.-M. Fan, A. Quiñones-Hinojosa, K. Konstantopoulos, *Nat. Biomed. Eng.* **2021**, *5*, 26.
- [19] R. H. Shoemaker, *Nat. Rev. Cancer* **2006**, *6*, 813.
- [20] B. Alday-Parejo, R. Stupp, C. Ruegg, *Cancers* **2019**, *12*, 11.
- [21] C. Bergonzini, K. Kroese, A. J. M. Zweemer, E. H. J. Danen, *Front. Cell Dev. Biol.* **2022**, *10*, 863850.
- [22] T. Koltai, *F1000Res* **2015**, *4*, 9.
- [23] M. Rudzińska, C. Daglioglu, L. V. Savvateeva, F. N. Kaci, R. Antoine, A. A. Zamyatinjr, *Drug Des. Devel. Ther.* **2021**, *15*, 9.
- [24] J. Huang, L. Zhang, D. Wan, L. Zhou, S. Zheng, S. Lin, Y. Qiao, *Signal Transduction Target Ther.* **2021**, *6*, 153.
- [25] E. Henke, R. Nandigama, S. Ergün, *Front. Mol. Biosci.* **2019**, *6*, 160.
- [26] S. J. Altschuler, L. F. Wu, *Cell* **2010**, *141*, 559.
- [27] B. Carter, K. Zhao, *Nat. Rev. Genet.* **2021**, *22*, 235.
- [28] C. E. Meacham, S. J. Morrison, *Nature* **2013**, *501*, 328.
- [29] N. Mcgranahan, C. Swanton, *Cell* **2017**, *168*, 613.
- [30] J. S. You, P. A. Jones, *Cancer Cell* **2012**, *22*, 9.
- [31] A. Torgovnick, B. Schumacher, *Front. Genet.* **2015**, *6*, 157.
- [32] T. L. Whiteside, *Oncogene* **2008**, *27*, 5904.
- [33] I. Dagogo-Jack, A. T. Shaw, *Nat. Rev. Clin. Oncol.* **2018**, *15*, 81.
- [34] P. R. Prasetyanti, J. P. Medema, *Mol. Cancer* **2017**, *16*, 41.
- [35] L. G. Rodriguez, X. Wu, J. L. Guan, *Methods Mol. Biol.* **2005**, *294*, 23.
- [36] H. C. Chen, *Methods Mol. Biol.* **2005**, *294*, 15.
- [37] Y. Xie, W. Zhang, L. Wang, K. Sun, Y. Sun, X. Jiang, *Lab Chip* **2011**, *11*, 2819.
- [38] D. Irimia, G. Charras, N. Agrawal, T. Mitchison, M. Toner, *Lab Chip* **2007**, *7*, 1783.
- [39] M. K. Shin, S. K. Kim, H. Jung, *Lab Chip* **2011**, *11*, 3880.
- [40] J. Yan, D. Irimia, *Technology* **2014**, *2*, 185.
- [41] S. Bajpai, M. J. Mitchell, M. R. King, C. A. Reinhart-King, *Technology* **2014**, *2*, 101.
- [42] D. Irimia, M. Toner, *Integr. Biol.* **2009**, *1*, 506.
- [43] M. Mak, C. A. Reinhart-King, D. Erickson, *PLoS One* **2011**, *6*, e20825.
- [44] D. Gallego-Perez, N. Higuera-Castro, L. Denning, J. Dejesus, K. Dahl, A. Sarkar, D. J. Hansford, *Lab Chip* **2012**, *12*, 4424.
- [45] Y.-G. Ko, C. C. Co, C.-C. Ho, *Soft Matter* **2013**, *9*, 2467.
- [46] R. Dent, M. Trudeau, K. I. Pritchard, W. M. Hanna, H. K. Kahn, C. A. Sawka, L. A. Lickley, E. Rawlinson, P. Sun, S. A. Narod, *Clin. Cancer Res.* **2007**, *13*, 4429.
- [47] S. Al-Mahmood, J. Sapiezynski, O. B. Garbuzenko, T. Minko, *Drug Delivery Transl. Res.* **2018**, *8*, 1483.
- [48] M. Venere, C. Horbinski, J. F. Crish, X. Jin, A. Vasanji, J. Major, A. C. Burrows, C. Chang, J. Prokop, Q. Wu, P. A. Sims, P. Canoll, M. K. Summers, S. S. Rosenfeld, J. N. Rich, *Sci. Transl. Med.* **2015**, *7*, 304ra143.
- [49] L. Cayetano-Salazar, M. Olea-Flores, M. D. Zuñiga-Eulogio, C. Weinstein-Opppenheimer, G. Fernández-Tilapa, M. A. Mendoza-Catalán, A. E. Zacapala-Gómez, J. Ortiz-Ortiz, C. Ortuño-Pineda, N. Navarro-Tito, *Phytother. Res.* **2021**, *35*, 4092.
- [50] K. K. L. Chan, M. K. Y. Siu, Y.-X. Jiang, J.-J. Wang, T. H. Y. Leung, H. Y. S. Ngan, *Cancer Cell Int.* **2018**, *18*, 65.
- [51] F. Tang, P. Hu, Z. Yang, C. Xue, J. Gong, S. Sun, L. Shi, S. Zhang, Z. Li, C. Yang, J. Zhang, C. Xie, *Oncol. Rep.* **2017**, *37*, 3449.
- [52] H. Ha, B. Debnath, N. Neamati, *Theranostics* **2017**, *7*, 1543.
- [53] M. Muñoz, A. González-Ortega, M. V. Salinas-Martín, A. S. Carranza, S. Garcia-Recio, V. Almendro, R. Coveñas, *Int. J. Oncol.* **2014**, *45*, 1658.
- [54] L. Kubiczikova, L. Pour, L. Sedlarikova, R. Hajek, S. Sevcikova, *J. Cell. Mol. Med.* **2014**, *18*, 947.
- [55] C.-J. Lai, R. Bao, X. u Tao, J. Wang, R. Atoyan, H. Qu, D. a-G. Wang, L. Yin, M. Samson, J. Forrester, B. Zifcak, G.-X. Xu, S. Dellarocca, H.-X. Zhai, X. Cai, W. E. Munger, M. Keegan, C. V. Pepicelli, C. Qian, *Cancer Res.* **2010**, *70*, 3647.
- [56] B. Al-Lazikani, U. Banerji, P. Workman, *Nat. Biotechnol.* **2012**, *30*, 679.
- [57] V. Vasioukhin, C. Bauer, M. Yin, E. Fuchs, *Cell* **2000**, *100*, 209.
- [58] J. R. Davis, A. Luchici, F. Mosis, J. Thackery, J. A. Salazar, Y. Mao, G. A. Dunn, T. Betz, M. Miodownik, B. M. Stramer, *Cell* **2015**, *161*, 361.
- [59] H. Zhang, J. S. Berg, Z. Li, Y. Wang, P. Lång, A. D. Sousa, A. Bhaskar, R. E. Cheney, S. Strömblad, *Nat. Cell Biol.* **2004**, *6*, 523.
- [60] I. Miller, M. Min, C. Yang, C. Tian, S. Gookin, D. Carter, S. L. Spencer, *Cell Rep.* **2018**, *24*, 1105.
- [61] E. Neubauer, R. M. Wirtz, D. Kaemmerer, M. Athelougo, L. Schmidt, J. SÄ×Nger, A. Lupp, *Oncotarget* **2016**, *7*, 41959.
- [62] A. S. Nikonova, I. Astsaturov, I. G. Serebriiskii, R. L. Dunbrack, E. A. Golemis, *Cell. Mol. Life Sci.* **2013**, *70*, 661.
- [63] Y. Fang, H. Yu, X. Liang, J. Xu, X. Cai, *Cancer Biol. Ther.* **2014**, *15*, 1268.
- [64] J. Liu, L. Min, S. Zhu, Q. Guo, H. Li, Z. Zhang, Y. u Zhao, C. Xu, S. Zhang, *J. Cancer* **2019**, *10*, 1915.
- [65] J. E. Noll, K. Vandyke, D. R. Hewett, K. M. Mrozik, R. J. Bala, S. A. Williams, C. H. Kok, A. C. Zannettino, *J. Hematol. Oncol.* **2015**, *8*, 106.
- [66] R. A. Battaglia, S. Delic, H. Herrmann, N. T. Snider, *F1000 Res* **2018**, *7*, 1796.
- [67] M. Raftopoulou, A. Hall, *Dev. Biol.* **2004**, *265*, 23.
- [68] A. J. Ridley, *Curr. Opin. Cell Biol.* **2015**, *36*, 103.

- [69] N. Xu, G.-Y. Qu, Y.-P. Wu, Y.-Z. Lin, D.-N. Chen, X.-D. Li, S.-H. Chen, J.-B. Huang, Q.-S. Zheng, X.-Y. Xue, Y. Wei, *J. Cell. Biochem.* **2020**, *121*, 231.
- [70] K. O'connor, M. Chen, *Small GTPases* **2013**, *4*, 141.
- [71] F. M. Vega, G. Fruhwirth, T. Ng, A. J. Ridley, *J. Cell Biol.* **2011**, *193*, 655.
- [72] S. G. Allen, Y.-C. Chen, J. M. Madden, C. L. Fournier, M. A. Altemus, A. B. Hiziroglu, Y.-H. Cheng, Z. F. Wu, L. Bao, J. A. Yates, E. Yoon, S. D. Merajver, *Sci. Rep.* **2016**, *6*, 39190.
- [73] H. Katoh, K. Hiramoto, M. Negishi, *J. Cell Sci.* **2006**, *119*, 56.
- [74] K. A. Makowska, R. E. Hughes, K. J. White, C. M. Wells, M. Peckham, *Cell Rep.* **2015**, *13*, 2118.
- [75] B. A. Humphries, J. M. Buschhaus, Y.-C. Chen, H. R. Haley, T. Qyli, B. Chiang, N. Shen, S. Rajendran, A. Cutter, Y.-H. Cheng, Y.-T. Chen, J. Cong, P. C. Spinosa, E. Yoon, K. E. Luker, G. D. Luker, *Mol. Cancer Res.* **2019**, *17*, 1142.
- [76] K. Ishizawa, Z. A. Rasheed, R. Karisch, Q. Wang, J. Kowalski, E. Susky, K. Pereira, C. Karamboulas, N. Moghal, N. V. Rajeshkumar, M. Hidalgo, M. Tsao, L. Ailles, T. K. Waddell, A. Maitra, B. G. Neel, W. Matsui, *Cell Stem Cell* **2010**, *7*, 279.
- [77] Z. Yu, T. G. Pestell, M. P. Lisanti, R. G. Pestell, *Int. J. Biochem. Cell Biol.* **2012**, *44*, 2144.
- [78] E. Vlashi, F. Pajonk, *Semin. Cancer Biol.* **2015**, *31*, 28.
- [79] I. A. Silva, S. Bai, K. Mclean, K. Yang, K. Griffith, D. Thomas, C. Ginestier, C. Johnston, A. Kueck, R. K. Reynolds, M. S. Wicha, R. J. Buckanovich, *Cancer Res.* **2011**, *71*, 3991.
- [80] E. M. Campoy, M. T. Branham, L. S. Mayorga, M. Roquã©, *BMC Cancer* **2019**, *19*, 328.
- [81] G. N. Khan, E. J. Kim, T. S. Shin, S. H. Lee, *Anticancer Res.* **2017**, *37*, 2343.
- [82] Y. Shen, B. U. S. Schmidt, H. Kubitschke, E. W. Morawetz, B. Wolf, J. A. Käs, W. Losert, *Cancer Convergence* **2020**, *4*, 1.
- [83] V. T. Devita, R. C. Young, G. P. Canellos, *Cancer* **1975**, *35*, 98.
- [84] D. A. Yardley, *Int. J. Breast Cancer* **2013**, *2013*, 137414.
- [85] R. Macarron, M. N. Banks, D. Bojanic, D. J. Burns, D. A. Cirovic, T. Garyantes, D. V. S. Green, R. P. Hertzberg, W. P. Janzen, J. W. Paslay, U. Schopfer, G. S. Sittampalam, *Nat. Rev. Drug Discov.* **2011**, *10*, 188.
- [86] J. Tang, L. Karhinen, T. Xu, A. Szwajda, B. Yadav, K. Wennerberg, T. Aittokallio, *PLoS Comput. Biol.* **2013**, *9*, e1003226.
- [87] Z. Zhang, L. Chen, B. Humphries, R. Brien, M. S. Wicha, K. E. Luker, G. D. Luker, Y.-C. Chen, E. Yoon, *Integr. Biol.* **2018**, *10*, 758.
- [88] Y.-H. Cheng, Y.-C. Chen, R. Brien, E. Yoon, *Lab Chip* **2016**, *16*, 3708.
- [89] Y.-C. Chen, Z. Zhang, E. Yoon, *Anal. Chem.* **2020**, *92*, 7717.
- [90] E. Z. Macosko, A. Basu, R. Satija, J. Nemeshe, K. Shekhar, M. Goldman, I. Tirosh, A. R. Bialas, N. Kamitaki, E. M. Martersteck, J. J. Trombetta, D. A. Weitz, J. R. Sanes, A. K. Shalek, A. Regev, S. A. Mccarroll, *Cell* **2015**, *161*, 1202.
- [91] T. M. Gierahn, M. H. Wadsworth, T. K. Hughes, B. D. Bryson, A. Butler, R. Satija, S. Fortune, J. C. Love, A. K. Shalek, *Nat. Methods* **2017**, *14*, 395.
- [92] Y.-H. Cheng, Y.-C. Chen, E. Lin, R. Brien, S. Jung, Y.-T. Chen, W. Lee, Z. Hao, S. Sahoo, H. M. Kang, J. Cong, M. Burness, S. Nagrath, M. S. Wicha, E. Yoon, *Nat. Commun.* **2019**, *10*, 2163.
- [93] Y. Hao, S. Hao, E. Andersen-Nissen, W. M. Mauck, S. Zheng, A. Butler, M. J. Lee, A. J. Wilk, C. Darby, M. Zager, P. Hoffman, M. Stoeckius, E. Papalexi, E. P. Mimitou, J. Jain, A. Srivastava, T. Stuart, L. M. Fleming, B. Yeung, A. J. Rogers, J. M. Mcelrath, C. A. Blish, R. Gottardo, P. Smibert, R. Satija, *Cell* **2021**, *184*, 3573.
- [94] G. Y. Di Veroli, C. Fornari, D. Wang, S. V. Mollard, J. L. Bramhall, F. M. Richards, D. I. Jodrell, *Bioinformatics* **2016**, *32*, 2866.
- [95] E. Y. Chen, C. M. Tan, Y. Kou, Q. Duan, Z. Wang, G. V. Meirelles, N. R. Clark, A. Ma'ayan, *BMC Bioinf.* **2013**, *14*, 128.